# Stereo-PIV Measurement of Turbulence Shear Stress in a Stirred Flow Mixer

**Chandra Shekhar[1], Koichi Nishino[2] and Yoshiyuki Iso[1]**

[1] Heat and Fluid Dynamics Laboratory, IHI Corporation, Yokohama, Japan
chandra_shekhar@ihi.co.jp

[2] Department of Mechanical Engineering, Yokohama National University, Yokohama, Japan

## ABSTRACT

The turbulence dissipation rate and turbulence shear stress are estimated inside a cylindrical, stirred flow mixer by carrying out Stereo PIV measurements in twelve vertical and three horizontal planes. The flow domain is vertically oriented, filled with the water. A commercially-available, three-blade impeller, HR-100, is used as the agitator. The impeller is mounted near the tip of a thin, rigid shaft, which is aligned along the central axis of the flow domain. The impeller rotates with the constant angular speed of 150RPM, and the Reynolds number based on the impeller diameter and the blade's tip-velocity is equal to 59400. The turbulence statistics in the vertical measurement planes are reported before (Shekhar C, Nishino K, Yamane Y and Huang J, "Stereo-PIV measurement of turbulence characteristics in a flow mixer" *Journal of Visualization* 15 (2012) pp.293~308), which revealed that the rotation induces a downward, as well as tangential, bulk flow motion, which convects the turbulence generated at the blade-water interface, causing the turbulence level below the impeller to be much higher than the level above it. The present study is the second part of the same project, and reports the turbulence statistics in the horizontal measurement planes. The results show that the turbulence level is high in the area swept by the rotating impeller blades and underneath. However, in the outside region, the turbulence damps down and becomes negligible. The vertical and horizontal measurement results are also combined to estimate the production, convection, viscous diffusion, and turbulence dissipation terms of the turbulence kinetic energy's budget equation, along with the turbulence shear stress, along the lines where the different vertical and horizontal planes intersect.

**Keywords:** Stirred mixer, Stereo PIV, turbulence, budget equation, dissipation rate, shear stress

## 1. INTRODUCTION

Turbulent flow mixers are widely used in various practical applications, starting from home appliances to medical applications and in large scale industrial mixers. In general, the mixers can be divided into passive and active mixers. The passive mixers usually consist of a static, rigid unit, which is inserted into a flow to enhance mixing in the wake region. The active mixers, on the other hand, happen to be dynamic, such as, an agitator, which imparts momentum to the flow in order to enhance the mixing. The most extensively used configuration of the active mixers is perhaps a rotating impeller inserted in a flow and driven by a motor.

In past, many attempts have been made to understand the flow properties of the rotating mixers, both numerically and experimentally, using different types of the impeller. Rao & Brodkey [1], Sharp & Adrian [2], and Ducci & Yianneskis [3] experimentally studied such a flow in a cylindrical tank, and found the turbulence being strongly anisotropic at practically measurable spatial scales, which has continuously been a major obstacle, till date. Researchers are often interested in estimating the turbulence dissipation rate and turbulence shear stress of the mixing flows. Many researchers have taken indirect approaches to resolve this problem. Delafosse et al [4] (who carried out two-dimensional PIV measurement using a Mixel TTP impeller) introduced the "so called" isotropic ratios, which is essentially a quantitative measure of the anisotropy present in the flow at the measured scale. Based on this, they proposed that the calculated turbulence dissipation rate should be reduced to 0.8 times, for the spatial scale achieved in their measurements. On the other hand, Baldi & Yianneskis [5] tried to directly measure the turbulence dissipation rate using PIV. They could achieve the spatial resolution of 0.1 mm, and found that their results matches well with some past results, but differ with many others at the same time.

Some researchers have tried to understand the flow properties by theoretically slicing the flow volume into many planes, and then carrying out separate measurements in all these planes. Yoon et al [6] carried out such an study by

## NOMENCLATURE

$D$ : Mean diameter of the HR-100 impeller, *90 mm*.

$Re$ : Reynolds number (defined as $\omega D^2/2\gamma$), *59400*.

$t$ : Time

$X$ : Horizontal axis in rightward direction, with the origin lying on the central axis of the measurement tank.

$Y$ : Vertical axis in upward direction, with the origin located on the central axis of the measurement tank, *400 mm* inside.

$Z$ : Direction perpendicular to the *X*-*Y* plane, considering a right-handed Cartesian coordinate system.

$u$ : *X*-component of the velocity.

$v$ : *Y*-component of the velocity.

$V_{uvw}$ : Magnitude of the absolute velocity; that is, $(u^2 + v^2 + w^2)^{0.5}$.

$w$ : *Z*-component of the velocity.

## GREEK ALPHABETS

$\gamma$ : Kinematic viscosity.

$\varepsilon$ : Turbulence dissipation rate per unit mass.

$\tau$ : Turbulence shear stress.

$\varphi$ : Phase angle, which defines the angular location of the vertical measurement plane.

$\omega$ : Impeller's rotation speed in clockwise direction, *150 RPM* (*15.7 rad/s*).

## ABBREVIATIONS

*RMS* : Root mean square value.

*RPM* : Revolutions per minute.

*RSS* : Reynolds shear stress; e.g. $RSS_{u'v'} \equiv \overline{u'v'}$ etc.

*TKE* : Turbulence kinetic energy $\equiv (\overline{u'u'} + \overline{v'v'} + \overline{w'w'})/2$.

## CONVENTIONS

$\langle a \rangle$ : Normalized value of any physical quantity, $a$.

$\bar{a}$ : Mean value of any physical quantity, $a$.

$a'$ : Turbulence fluctuation in any physical quantity, $a$.

$a_{RMS}$ : RMS of the turbulence fluctuations, $a'$.

using two-dimensional PIV technique in six axisymmetric planes, with the angular distance between any two adjacent planes being 10°. Their flow domain was a cylindrical tank, with a six-blade Rushton impeller as the agitator. Recently, Shekhar et al [7] carried out phase-synchronized, stereo PIV measurements inside a cylindrical tank (see Fig.1), with a commercially available, three-blade, HR-100 impeller [8] (see Fig.2) as the agitator. They presented the mean velocity, turbulence kinetic energy, and Reynolds shear stress at twelve different axisymmetric planes, separated with each-other by the constant angle of 10°, such that the whole 120° angular space between any two of the impeller-blades are covered. They found that each of the blades' tip generate a vortex with high level of turbulence. The impeller induced an up-to-down bulk flow motion, which pushed these vortices down, along with the turbulence generated by the blades. Moreover, the viscous drag caused the vortices to lag behind the blade's circumferential motion. In this process, the turbulence level inside the vortices gradually decreased, whereas its size became bigger. As a result, three helical,

discontinuous vortical pipes were created inside the flow domain, which rotated with the angular speed of blade, but bends in the opposite direction of the motion. The same experimental configuration (see Figs.2 and 3) as in this study is used even in the present study.

In the present study, which is the second part of the same measurement project, we have carried out phase-synchronized, stereo PIV measurements in three different horizontal planes below the impeller blades. Each of the horizontal measurement planes covers the whole 120° angular space between any two of the impeller blades. The obtained results are also combined with our previous, vertical plane measurement results to calculate the production, convection, and viscous diffusion terms of the turbulence kinetic energy's budget equations, along the lines where the vertical and horizontal planes intersect (see Fig.3). After neglecting the pressure diffusion and turbulence diffusion terms, the turbulence dissipation rate, as well as a representative value of the shear stress that a living tissue inside the working fluid would experience, is also estimated by substituting the aforementioned terms in the budget equation.

In the following of this paper, at first, the studied system and the PIV methodology are briefed in section 2. Although these are almost same as in our previous study, they are described for the completion purposes. In section 3, the mean velocity and turbulence statistics in the three horizontal measurement planes are presented. It is followed by a description of the strategy that is used to combined the vertical and horizontal measurement results, in order to compute the budget equation terms, followed by their plots along the 6 × 3 = 18 lines that result when 6 alternative vertical planes and the 3 horizontal planes intersect.

**Non-dimensionalization**

In the present study, all the physical quantities are presented in non-dimensional forms. The normalization procedure is kept same as in our previous study [7], to provide easy understanding of the overall measurement results. The spatial dimensions, the mean and the turbulence fluctuation components, and the turbulence kinetic energy and the Reynolds shear stress components are, respectively, non-dimensionalized with respect to the impeller diameter ($D$), the blade's tip velocity ($\omega D/2$), and square of the blade's tip velocity ($\omega^2D^2/4$), respectively. Similarly, the budget equation terms and the turbulence shear stress are normalized with respect to the quantities $\omega^3D^3/8D$ and $\sqrt{\omega^3 D^3/8D}$, respectively. All the non-dimensionalized quantities are presented in < >.

It should be noted that the Latin and Greek nomenclatures used in the present study are also kept consistent with the ones in our previous study [1].

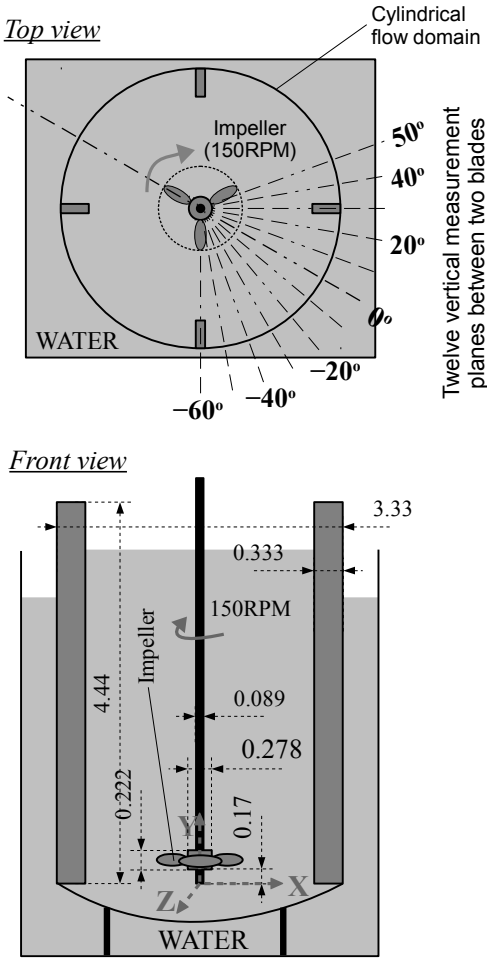


**Figure 1:** Schematic diagrams of the flow domain and the measurement planes. All the spatial dimensions are in non-dimensional form.

**Figure 2:** The HR-100 impeller, whose diameter, *D*, is equal to *90 mm*. It is used as the impeller in the present study.

## 2. SYSTEM DETAILS AND EXPERIMENTAL METHODOLOGY

The measurement system (see Fig.1, which also shows the Cartesian coordinate system used in the present study) consists of a cylindrical, vertical tank, with the water as the working fluid. The HR-100 impeller is mounted near the tip of a thin, round shaft, which is placed along the central axis of the tank, from up. The shaft is driven in clockwise direction with the angular speed of *150 RPM* (*15.7 rad/s*), using an electric motor. This motion induces an up to down bulk motion in the water, as well as some tangential motion. This tank is placed inside a larger, square tank, which is

also filled with water, in order to reduce the optical distortion when viewed from outside. The water is first deaerated, in order to remove tiny air bubbles that happen to exist inside tap water, by heating it until 60°C, and then used in the experiment after it naturally cools down to about 17°C. At this temperature, the blade's tip-velocity based Reynolds number is about 59400.

It should be noted that the cylindrical tank also has four narrow, equidistant baffle plates, which significantly enhances the mixing in the radially far regions, such as, near the cylindrical wall. These baffle plated are likely to induce only marginal asymmetry in the flow characteristics in the central region, which the region of interest in the present study. Therefore, angular orientation of the cylindrical tank is not taken into account when carrying out the measurements.

The horizontal flow measurements are carried out at the axial locations $\langle Y \rangle$ = 0.0556, 0.1667, and 0.3333, using the stereo PIV technique [9]. The overall experimental setup consists of (1) the water-filled cylindrical tank with the HR-100 impeller inside it, (2) the spherical Nylon particles of size 25 μm, to seed the flow, (3) two high-speed CCD cameras, (4) a double-pulse Nd:YAG laser system of 30 mJ/pulse energy output, (5) an optical system that converts the round laser beam into a thin, horizontal light sheet (6) a digital time-delay generator, (7) a precise, laser-based, phase-synchronization mechanism [7] to acquire the particle images exactly when a given blade of the rotating impeller reaches a given angular location, and (8) a computer to synchronize the electronic equipments and store the acquired particle images. All the experimental equipments, other than the rotating impeller, are fixed in space.

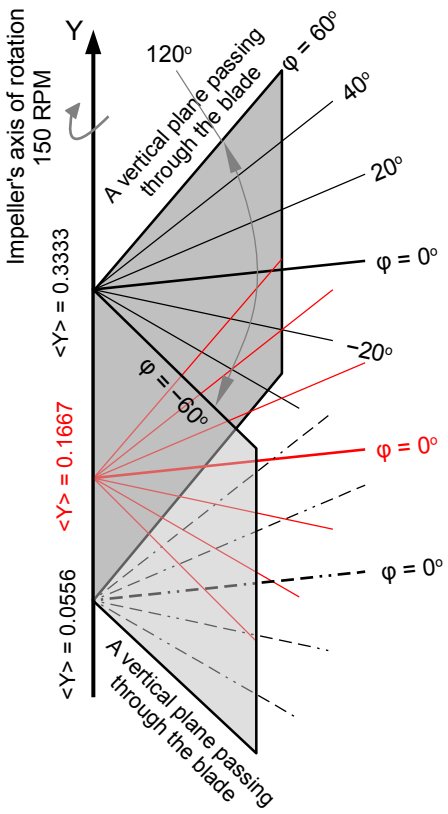


**Figure 3:** Three-dimensional view of the radial intersection lines where the turbulence dissipation energy and the turbulence shear stress are estimated.

The aforementioned laser-based phase-synchronization system consists of a small, continuous laser, a small mirror that reflects the continuous laser light, and a laser light detector embedded in the laser emitting device. The mirror is fixed perpendicular to the laser beam, at some distance from the emitting device, so that the detector received the reflected light. When a thin metal bar, which is fixed with the rotating shaft on which the impeller is mounted, passed through the space between the laser device and the mirror, it interrupts the light, which caused the laser device to transmit an electric signal to the digital delay generator, which receives it as the input signal and send further signals to the imaging, Nd:YAG laser and the CCD cameras, after some time delay. By manually controlling this time delay, a precise angular location of the rotating blades is achieved during the measurements.

The above system is used to obtain a total of 1000 pairs of the particle images of size 1600×1200 pixels in each of the vertical and horizontal planes. The horizontal-plane particle images are analyzed with the interrogation window size of 32×32 pixels, which is equivalent to 4×4 mm in the physical coordinate system. In the vertical plane measurements, the sizes of the tracer particles and the interrogation window were 8~12 μm and 1.5×1.5 mm, respectively. The resolution of the horizontal plane measurement is reduced in order to cover the whole 120° of the angular space between the impeller blades.

The 1000 pairs of the acquired particle images yield 1000 instantaneous velocity vector fields, which are used to calculate the mean velocity, turbulence statistics, and the budget equation terms along the intersection lines, which are shown in Fig.3. These lines result when the vertical planes at $\varphi$ = −60°, −40°, −20°, 0°, 20°, 40° intersect with the horizontal planes at $\langle Y \rangle$ = 0.0556, 0.1667, and 0.3333. Here, the angular location $\varphi$ = 0° lies in the middle of any two of the impeller-blades.

## 3. RESULTS AND DISCISSION

In this section, at first, the results obtained from the horizontal-plane measurements are presented, and then the budget equation terms and turbulence shear stress are estimated.

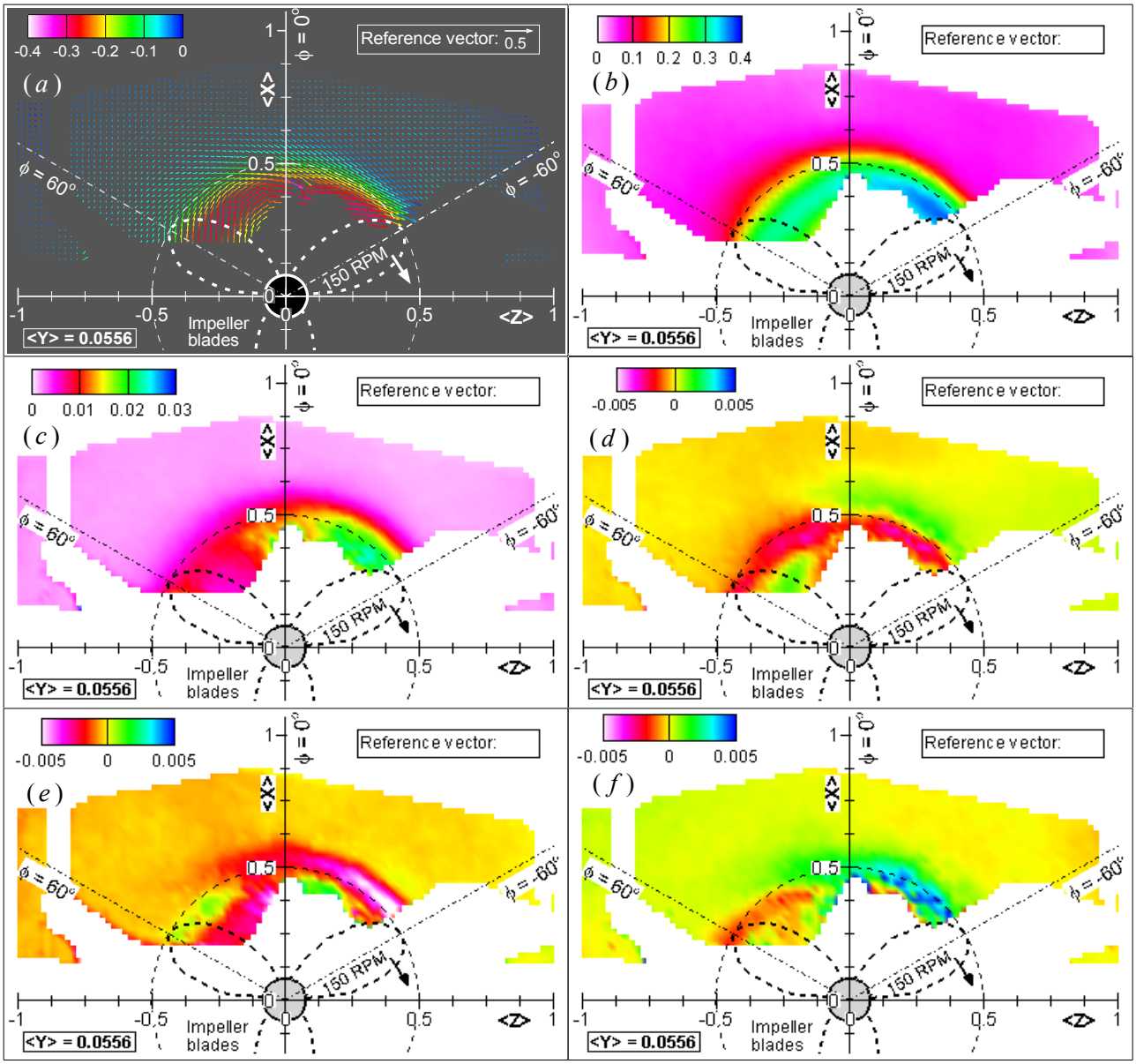


**Figure 4:** The (a) mean velocity vectors, with the vector colors showing the magnitude of the axial velocity component, (b) $\langle \overline{V}_{uvw} \rangle$, (c) $\langle TKE \rangle$, (d) $\langle RSS_{uv} \rangle$, (e) $\langle RSS_{vw} \rangle$, and (f) $\langle RSS_{wu} \rangle$ plots at $\langle Y \rangle$ = 0.0556.

### 3.1. Horizontal-plane results

The mean velocity vectors, $\langle \overline{V}_{uvw} \rangle$, $\langle TKE \rangle$, $\langle RSS_{uv} \rangle$, $\langle RSS_{vw} \rangle$, and $\langle RSS_{wu} \rangle$ in the $\langle Y \rangle$ = 0.0556, 0.1667, and 0.3333 planes are plotted in Figs.4, 5, and 6, respectively. In these plots, a representative view of the impeller blades is also drawn, in order to show the relative measurement region. However, the shape of the blades shown in the drawing significantly differ from the shape of the physical impeller blades. Therefore, the drawing should be perceived only in approximate sense. It should be further noted that the presented results also cover a small fraction of the area below the impeller blades, as these areas could be visualized due to angular orientation of the CCD cameras. On the other hand, a large section of the space between the impeller are not visualized, because the visual access was blocked by the blades and the impeller's hub.

The mean velocity plots clearly show the presence of a large vortex near the tip of the blades, which was also observed in the vertical plane measurements in our previous study [7]. The plots also demonstrate high overall mean flow velocity, high downward flow speed, and high turbulence level in the area swept by the rotating blades. Moreover, the Reynolds shear stress components are an order of magnitude smaller than the turbulence kinetic energy, and they

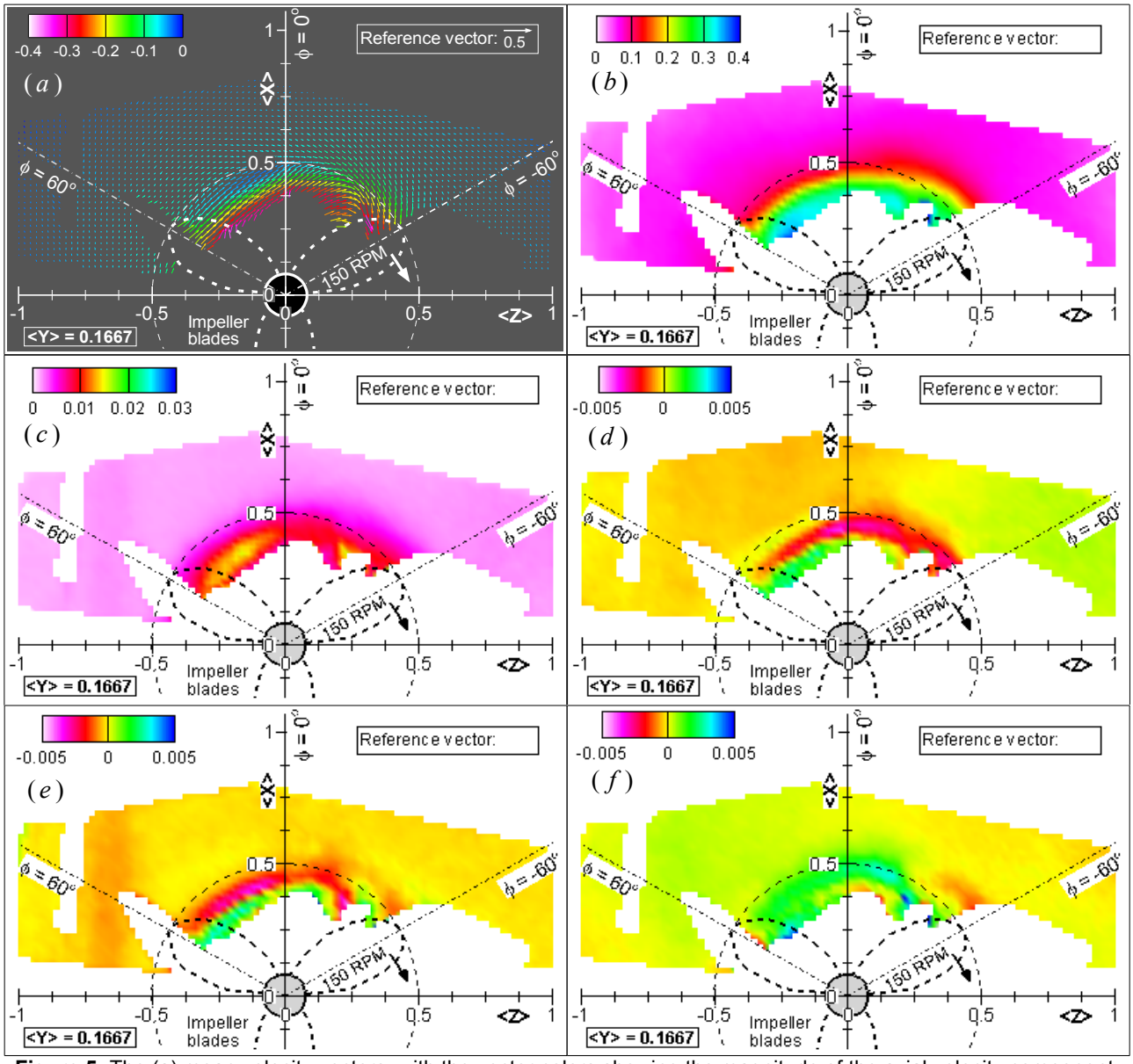


**Figure 5:** The (a) mean velocity vectors, with the vector colors showing the magnitude of the axial velocity component, (b) $\langle \overline{V}_{uvw} \rangle$, (c) $\langle TKE \rangle$, (d) $\langle RSS_{uv} \rangle$, (e) $\langle RSS_{vw} \rangle$, and (f) $\langle RSS_{wu} \rangle$ plots at $\langle Y \rangle = 0.1667$.

possess opposite signs in the $-60^o < \varphi < 0^o$ and $0^o < \varphi < 60^o$ regions.

The plots further show that the turbulence level at $\langle Y \rangle = 0.3333$ is smaller than the same in the lower horizontal planes (that is, in the planes at $\langle Y \rangle = 0.1667$ and $\langle Y \rangle = 0.0556$), perhaps because the turbulence generated at the blade-water interface is convected downward, fast, by the bulk flow motion. The mean velocity and turbulence level, both can also be observed to have become negligible outside the blade-swept region.

### 3.2. Budget equation terms of the turbulence kinetic energy and turbulence shear stress

*Production term:*

$$-\overline{u'u'}\cdot\frac{\partial \overline{u}}{\partial x} \quad \mathbf{-\overline{u'v'}\cdot\frac{\partial \overline{u}}{\partial y}} \quad -\overline{u'w'}\cdot\frac{\partial \overline{u}}{\partial z}$$
$$-\overline{v'u'}\cdot\frac{\partial \overline{v}}{\partial x} \quad -\overline{v'v'}\cdot\frac{\partial \overline{v}}{\partial y} \quad -\overline{v'w'}\cdot\frac{\partial \overline{v}}{\partial z}$$
$$-\overline{w'u'}\cdot\frac{\partial \overline{w}}{\partial x} \quad \mathbf{-\overline{w'v'}\cdot\frac{\partial \overline{w}}{\partial y}} \quad -\overline{w'w'}\cdot\frac{\partial \overline{w}}{\partial z}$$

*Convection term:*

$$-\overline{u}\cdot\frac{\partial (TKE)}{\partial x} \quad \mathbf{-\overline{v}\cdot\frac{\partial (TKE)}{\partial y}} \quad -\overline{w}\cdot\frac{\partial (TKE)}{\partial z}$$

*Viscous diffusion term:*

$$\gamma\cdot\frac{\partial^2 (TKE)}{\partial x^2} \quad \mathbf{+\gamma\cdot\frac{\partial^2 (TKE)}{\partial y^2}} \quad +\gamma\cdot\frac{\partial^2 (TKE)}{\partial z^2}$$

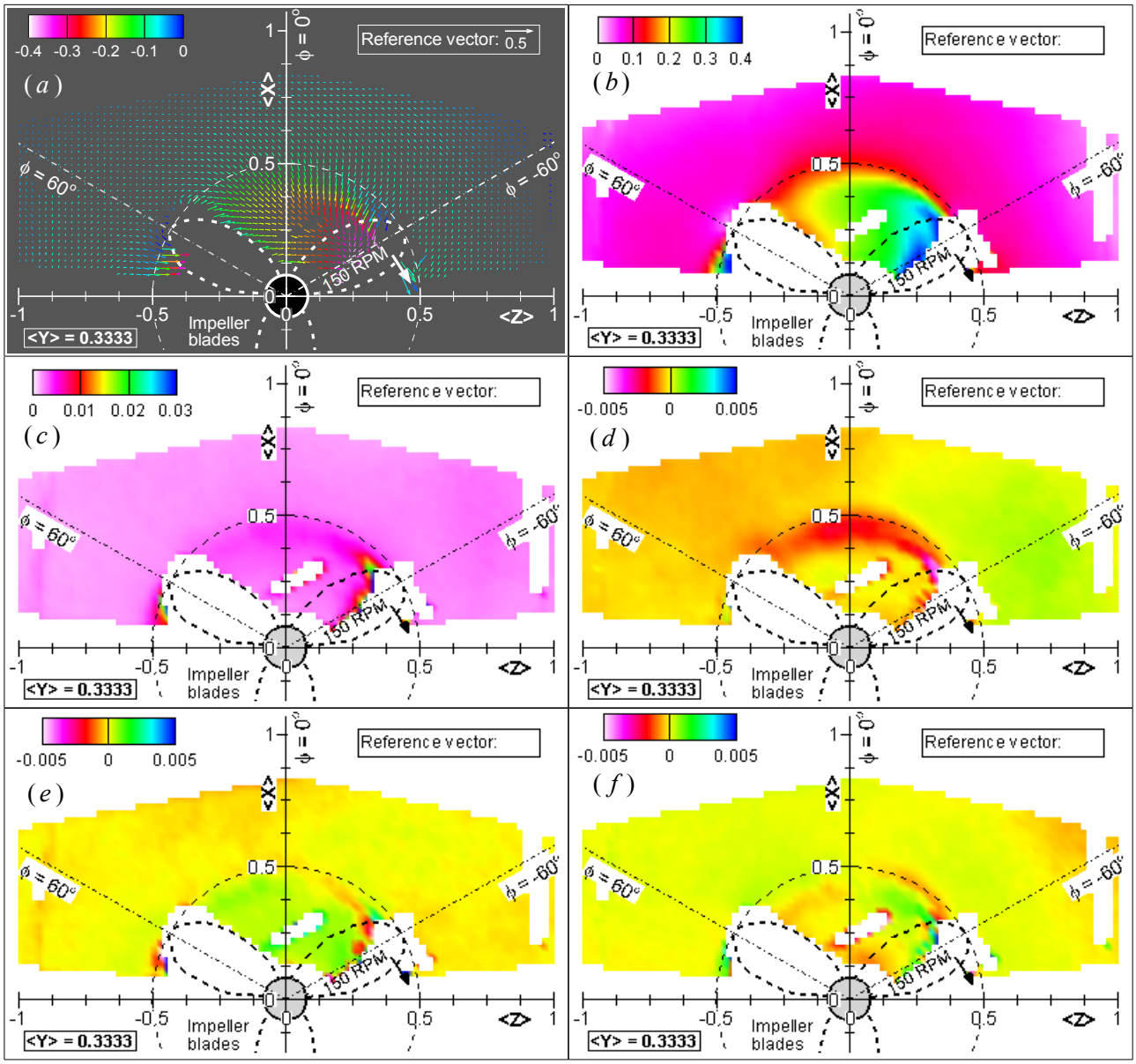


**Figure 6:** The (a) mean velocity vectors, with the vector colors showing the magnitude of the axial velocity component, (b) $\langle \overline{V}_{uvw} \rangle$, (c) $\langle TKE \rangle$, (d) $\langle RSS_{uv} \rangle$, (e) $\langle RSS_{vw} \rangle$, and (f) $\langle RSS_{wu} \rangle$ plots at $\langle Y \rangle$ = 0.3333.

The production, convection, viscous diffusion, and turbulence dissipation terms of the turbulence kinetic energy's budget equation are presented above. These are evaluated along the intersection lines shown in Fig.3. The terms represented in the bold letters are evaluated from the vertical plane measurement results, whereas the others are evaluated from the horizontal plane measurement results. Afterwards, the following equality is utilized to evaluate the turbulence dissipation term, as the residual of the budget equation after neglecting the pressure diffusion and turbulence diffusion terms.

*Turbulence dissipation, ε = Production + Convection + Viscous diffusion* …. (E1)

The obtained turbulence dissipation rate is used to derive a mean, representative value of the turbulence shear stress, by using the following equation:

$$\langle \bar{\tau} \rangle = \sqrt{2\langle \epsilon \rangle} \quad \cdots \quad \text{(E2)}$$

The right-handed, Cartesian coordinate system is used to calculate the budget equation terms, with the horizontal, *X* axis always aligning the intersection lines of the planes (see Fig.3). The vertical, *Y* axis, however, is fixed and always aligned along the central axis in the upward direction. The third, *Z* axis always is normal to the *X*-*Y* plane, in the right-

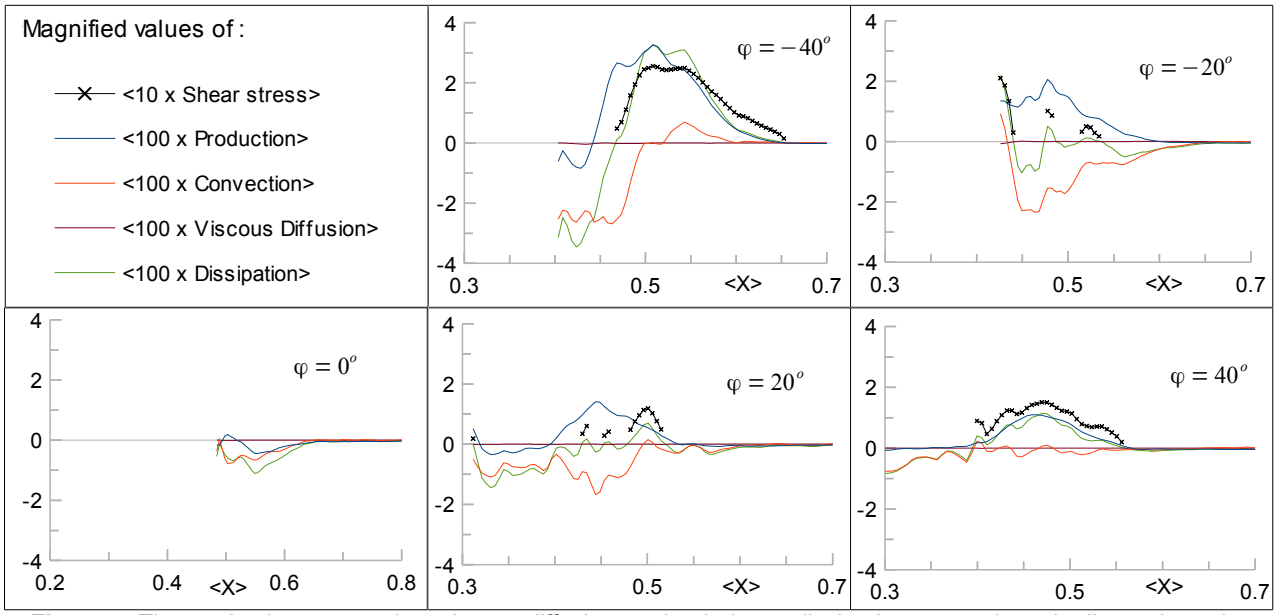


**Figure 7:** The production, convection, viscous diffusion, and turbulence dissipation terms along the lines where the vertical planes $\varphi$ = −40°, −20°, 0°, 20°, and 40° intersect with the horizontal plane <*Y*> = 0.0556.

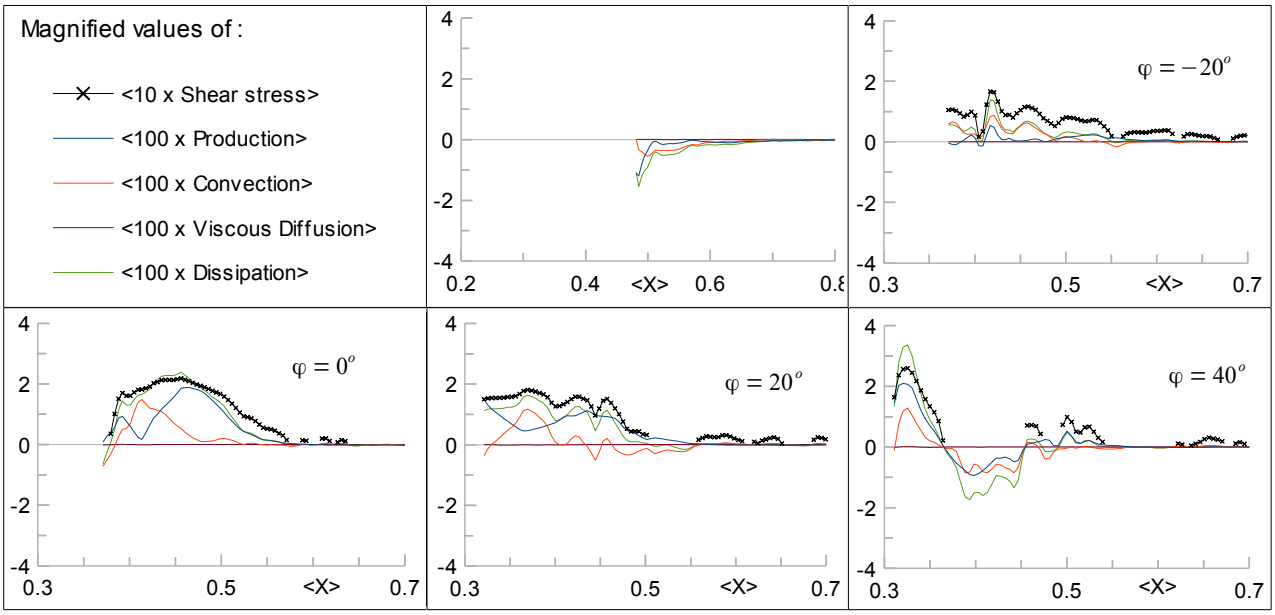


**Figure 8:** The production, convection, viscous diffusion, and turbulence dissipation terms along the lines where the vertical planes $\varphi$ = −40°, −20°, 0°, 20°, and 40° intersect with the horizontal plane <*Y*> = 0.1667.

handed way. The vertical plane measurement results in our previous study [7] also follow this conventions. However, the horizontal plane results in Figs. 4, 5, and 6 are presented in a fixed coordinate system where the X axis always lies along the $\varphi = 0^o$ line (and perpendicular to the central axis). Therefore, in order to combine the vertical and horizontal measurement results to compute the budget equation terms, the horizontal measurement results are rotated about the central axis by appropriate angles, so that the different $\varphi$ planes align along the $X$ axis. For this purpose, the following equations are derived, which rotates the horizontal measurement results in the counter-clockwise direction by an arbitrary angle $\theta$ (or, the coordinate system in the clockwise direction by the same angle):

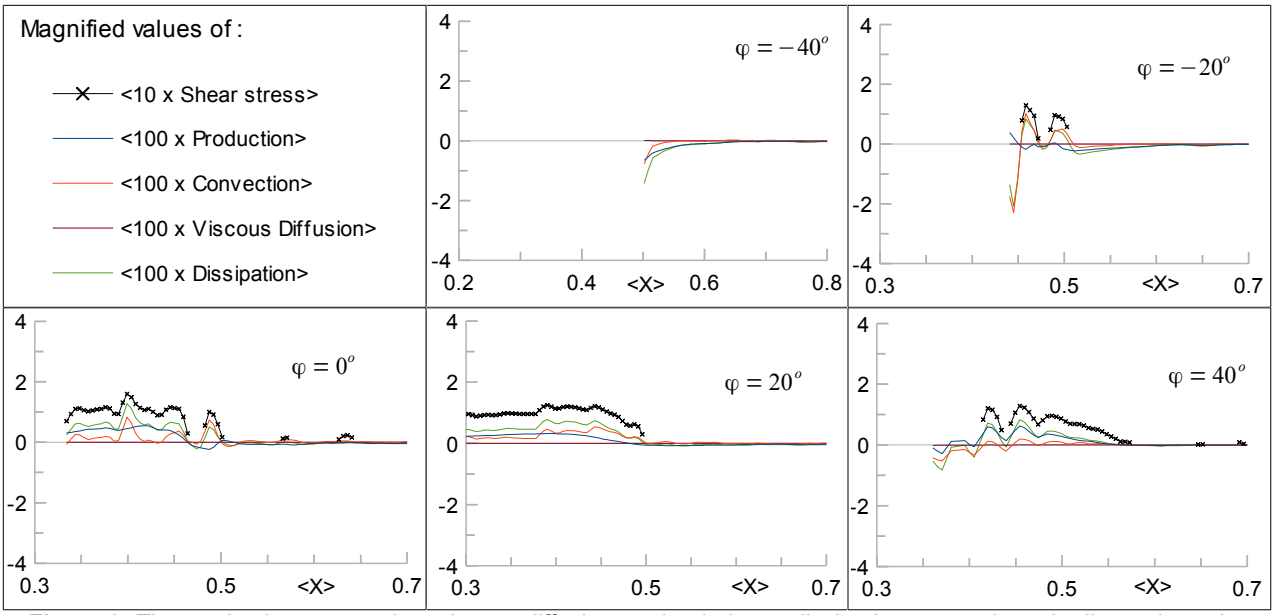


**Figure 9:** The production, convection, viscous diffusion, and turbulence dissipation terms along the lines where the vertical planes $\varphi$ = −40°, −20°, 0°, 20°, and 40° intersect with the horizontal plane <*Y*> = 0.3333.

$$Z = Z_0 \cos\theta - X_0 \sin\theta$$

$$X = Z_0 \sin\theta + X_0 \cos\theta$$

$$Y = Y_0$$

Here, the quantities with the subscript "0" represent the original results shown in the Figs.4, 5, and 6; and the non-subscript quantities represent the results after they are rotated by the angle $\theta$ (in the counter-clockwise direction).

Since the angular velocity of the reference frame is zero, the above relations can be differentiated with time to obtain the following:

$$w \equiv \frac{\partial Z}{\partial t} = w_0 \cos\theta - u_0 \sin\theta$$
$$u \equiv \frac{\partial X}{\partial t} = w_0 \sin\theta + u_0 \cos\theta$$
$$v \equiv \frac{\partial X}{\partial t} = v_0$$

These relations are used to derive the following turbulence quantities:

$$w'^2_{RMS} = w'^2_{0,RMS} \cos^2\theta + u'^2_{0,RMS} \sin^2\theta - RSS_{w'_0 u'_0} \sin 2\theta$$

$$u'^2_{RMS} = w'^2_{0,RMS} \sin^2\theta + u'^2_{0,RMS} \cos^2\theta + RSS_{w'_0 u'_0} \sin 2\theta$$

$$v'_{RMS} = v'_{0,RMS}$$

$$TKE = TKE_0$$

$$RSS_{u'v'} = RSS_{v'_0 w'_0} \sin\theta + RSS_{u'_0 v'_0} \cos\theta$$

$$RSS_{v'w'} = RSS_{v'_0 w'_0} \cos\theta - RSS_{u'_0 v'_0} \sin\theta, \text{ and}$$

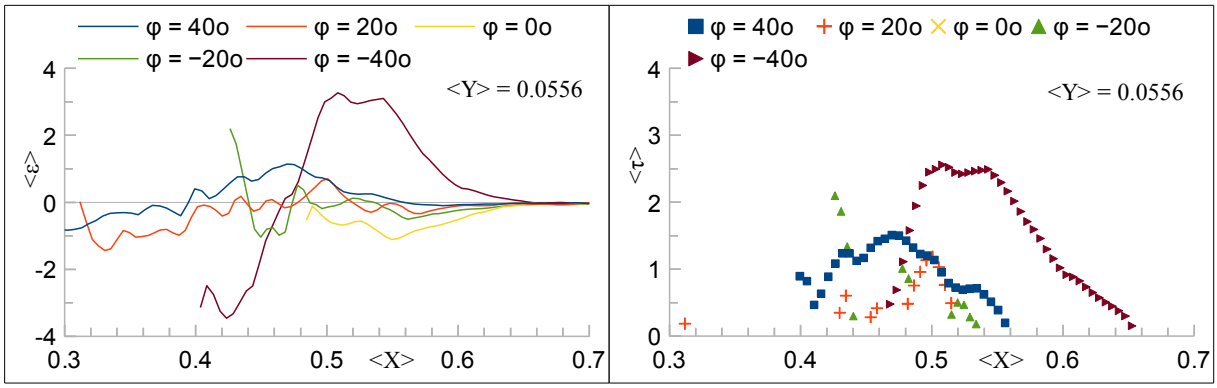


**Figure 10:** Turbulence dissipation rate and shear stress plots at the different phase angles in the <*Y*> = 0.0556 horizontal plane.

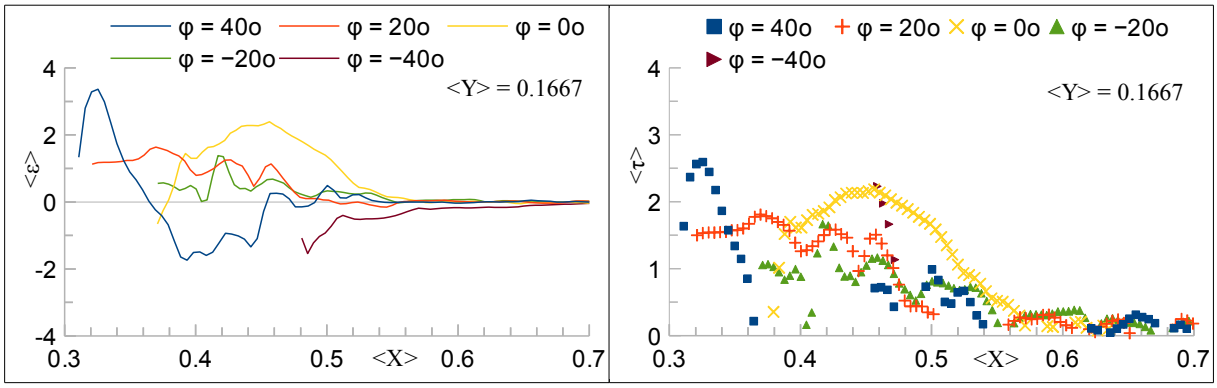


**Figure 11:** Turbulence dissipation energy and shear stress plots at the different phase angles in the <*Y*> = 0.1667 horizontal plane.

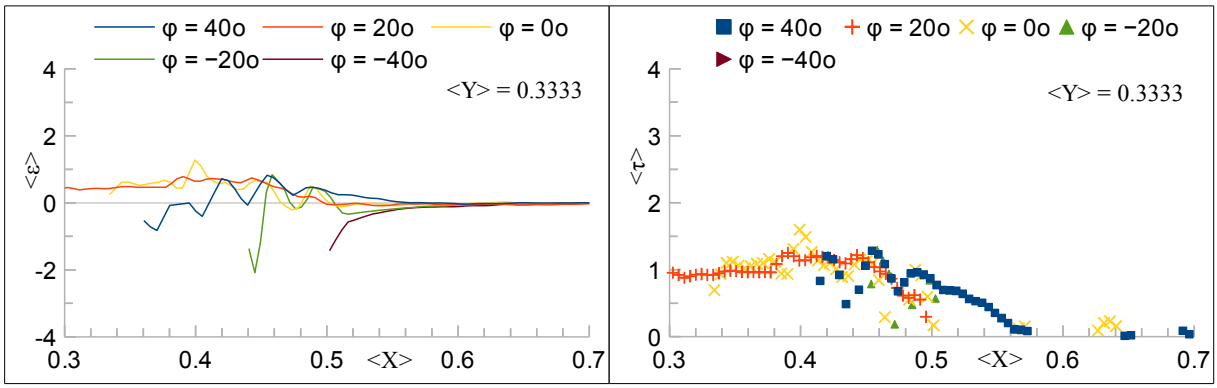


**Figure 12:** Turbulence dissipation energy and shear stress plots at the different phase angles in the <*Y*> = 0.3333 horizontal plane.

$$RSS_{w'u'} = \frac{1}{2}\left(w'^2_{RMS} - u'^2_{RMS}\right)\sin 2\theta + RSS_{w'_0u'_0}\cos 2\theta$$

In the above equations, the terms $w'^2_{RMS}$ etc represent the square of the quantities $w'_{RMS}$ etc.

When $\theta$ is set equal to the phase angles of a vertical measurement plane, the post-rotation horizontal plane results along the $X$ axis will become consistent with the same vertical plane results; and, therefore, the two can be combined to evaluate the budget equation terms. For example, if $\theta = 20^o$, the rotated results, along the $X$ axis, can be combined with the results obtained from the flow measurement in the vertical plane which is defined by $\varphi = -20^o$. Similarly, if $\theta = -20^o$, the results new results along the $X$ axis can be combined with the flow measurement results in the $\varphi = +20^o$

vertical plane.

It should be noted that the energy budget equation terms are evaluated at the locations which are common in both the vertical and horizontal plane measurements. As some flow regions are blocked by the blades and could not be visualized during the measurements, the spatial range of the budget equation calculations also differ with the axial and angular locations of the measurement planes. In fact, the common measurement locations do not exist at all along the $\varphi = -60^o$ line (see Fig.3); therefore, the calculations are not performed at this phase angle.

The calculated budget equation terms, along with the shear stress, are plotted along the intersection lines in the three horizontal measurement planes (which are defined by $<Y> = 0.0556$, 0.1667, and 0.3333) in Figs. 7, 8, and 9, respectively. Each of these figures contains the plots in the non-dimensional forms along the lines $\varphi = -40^o$, $-20^o$, $0^o$, $20^o$, and $40^o$. Moreover, the calculated equation terms are amplified 100 times, and the shear stresses are amplified 10 times, for the clarity purposes. The plots readily demonstrate that the viscous diffusion rate is negligible in all the cases. Moreover, inside the blade-swept area, the turbulence production rate is positive at most of the locations, but sometimes it becomes negative. Simultaneously, (1) the magnitudes of production and convection rates can be observed to be comparable with each other, (2) the magnitudes at the $<Y> = 0.3333$ location is smaller than the same at the lower horizontal planes, and (3) the budget equation terms tend to vanish in the region lying outside the blade-swiped area, indicating that the turbulence greatly damps down in this region. All these observations are consistent with the horizontal measurement results presented before in the Figs.4, 5, and 6.

The turbulence dissipation rates and turbulence shear stress at the different phase angles are separately discussed by plotting them together in the horizontal planes $<Y> = 0.0556$, 0.1667, and 0.3333, in Figs.10, 11, and 12, respectively, to provide an understanding of the way these quantities change with the phase angles. These plots are also respectively magnified by 100 and 10 times, respectively, which are same as when plotted in Figs.7, 8, and 9. The plots for the turbulence dissipation rate show that the calculated results are negative some times (which means that the turbulence energy is produced), although the physics of turbulent flows dictate that it should always be positive. This difference is likely due to neglecting the pressure and turbulence diffusion terms in the budget equation. Therefore, the obtained results are not suitable for the scientific purposes, but they may be useful in designing industrial applications. The negative values of the dissipation rate also prevent usage of the equation (E2) to evaluate the turbulence shear stress. Therefore, the shear stress are evaluated only at the locations where the dissipation rate is positive.

Both the turbulence diffusion and shear stress plots show that their magnitudes at $<Y> = 0.3333$ is smaller than the same at the downward locations. Moreover, their magnitudes, overall, is large in the blade-swept area, but become negligible in the outside region. These observations are consistent with the preceding observations. Moreover, when the plots at $\varphi = -40^o$ and $-20^o$ are compared with the plots at $\varphi = 20^o$ and $40^o$, it becomes evident that that the dissipation rate and shear stress are large in the immediate wake of the blades, but they reduce after some time when the turbulence damps down.

## CONCLUSIONS

Stereo-PIV measurements are carried out in three horizontal planes of a turbulent flow mixers, with the HR-100 impeller as the impeller and water as the working fluid. The results show that the mean velocity and turbulence level are significantly high in the area swept by the rotating impeller, but they are negligible in the outside regions. The turbulence level is also large in the region below the rotating impeller, perhaps because the turbulence generated at the blade-water interface is convected fast in the downward direction by the bulk motion of the flow. The turbulence level is also found to be high in the immediate wake of the moving blades, but it damps down after some time.

The present measurement results are combined with a previous measurement result where the stereo PIV measurements were carried in different vertical, axisymmetric planes, in order to estimate the production, convection, viscous diffusion, and turbulence dissipation terms of the energy budget equation. All these terms are high at the locations of high turbulence, except the viscous diffusion term which remains negligible everywhere. The viscous diffusion term is further used to estimate a representative value of the turbulence shear stress, which follows the same trend as the turbulence dissipation rate does.

## REFERENCES

[1] Rao MA, Brodkey RS “Continuous flow stirred tank turbulence parameters in the impeller stream” Chemical Engineering Science 27 (1972) pp.137~156.

[2] Sharp K, Adrian R “PIV study of small-scale structures around a Rushton turbine” AlChE Journal 47 (2001) pp.766~778.

[3] Ducchi A, Yianneskis M “Direct determination of energy dissipation in stirred vessels with two-point LDA” AlChE Journal 51 (2005) pp.2133~2149.

[4] Delafosse A, Collignon ML, Crine M, Toye D “Estimation of the turbulent kinetic energy dissipation rate from 2D-PIV measurements in a vessel stirred by an axial Mixel TTP impeller” Chemical Engineering Science 66 (2011) pp.1728~1737.

[5] Baldi S, Yianneskis M “On the quantification of energy dissipation in the impeller stream of a stirred vessel from fluctuating velocity gradient measurements” Chemical Engineering Science 59 (2004) pp.2659~2671.

[6] Yoon HS, Sharp KV, Hill DF, Adrian RJ, Balachandar S, Ha MY, Kar K “Integrated experimental and computational approach to simulation of flow in a stirred tank” Chemical Engineering Science 56 (2001) pp.6635–6649.

[7] Shekhar C, Nishino K, Yamane Y and Huang J “Stereo-PIV measurement of turbulence characteristics in a flow mixer” Journal of Visualization 15 (2012) pp.293~308.

[8] HR-100 impeller is manufactured by *Satake Chemical Equipment Ltd., Japan (*http://www.satake.co.jp/English*)*.

[9] Doorne CWH, Westerweel J “Measurement of laminar, transitional and turbulent pipe flow using Stereoscopic-PIV” Experiments in Fluids 42 (2007) pp.259~279.